THE JOURNAL OF PHYSICAL CHEMISTRY Letters

Letter

Cite This: J. Phys. Chem. Lett. 2018, 9, 647−653

pubs.acs.org/JPCL

Direct Observation of a Transiently Formed Isomer During Iodoform Photolysis in Solution by Time-Resolved X-ray Liquidography

Chi Woo Ahn,[†,‡] Hosung Ki,[‡] Joonghan Kim,[§] Jeongho Kim,[∥] Sungjun Park,[†,‡] Yunbeom Lee,[†,‡] Kyung Hwan Kim,[‡,∇] Qingyu Kong,[⊥] Jiwon Moon,[§] Martin Nors Pedersen,[#] Michael Wulff,[#] and Hyotcherl Ihee*[,†,‡]

[†]Department of Chemistry, Korea Advanced Institute of Science and Technology (KAIST), Daejeon 305-701, Republic of Korea

[‡]Center for Nanomaterials and Chemical Reactions, Institute for Basic Science (IBS), Daejeon, 34141, Republic of Korea

[§]Department of Chemistry, The Catholic University of Korea, Bucheon, 14662, Republic of Korea

[∥]Department of Chemistry and Chemical Engineering, Inha University, 100 Inha-ro, Nam-gu, Incheon, 22212, Republic of Korea

[⊥]Soleil synchrotron, Saint-Aubin, 91192, France

[#]European Synchrotron Radiation Facility (ESRF), 38000 Grenoble Cedex 9, France

Supporting Information

ABSTRACT: Photolysis of iodoform (CHI_3) in solution has been extensively studied, but its reaction mechanism remains elusive. In particular, *iso*-iodoform (*iso*-CHI_2−I) is formed as a product of the photolysis reaction, but its detailed structure is not known, and whether it is a major intermediate species has been controversial. Here, by using time-resolved X-ray liquidography, we determined the reaction mechanism of CHI_3 photodissociation in cyclohexane as well as the structure of *iso*-CHI_2−I. Both *iso*-CHI_2−I and CHI_2 radical were found to be formed within 100 ps with a branching ratio of 40:60. Iodine radicals (I), formed during the course of CHI_3 photolysis, recombine nongeminately with either CHI_2 or I. Based on our structural analysis, the I−I distance and the C−I−I angle of *iso*-CHI_2−I were determined to be 2.922 ± 0.004 Å and 133.9 ± 0.8°, respectively.

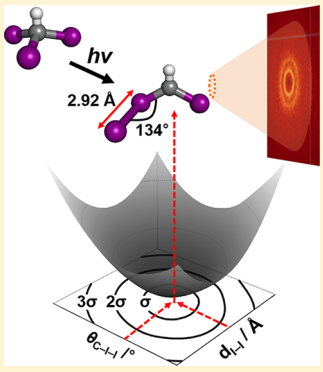

Photochemistry of polyhalomethanes has been extensively studied, due to their halogen-releasing properties, with a focus on reaction dynamics and structural rearrangement upon carbon−halogen bond cleavage.[1−8] The well-known photoreaction of these compounds is the formation of so-called "*iso*-polyhalomethane" species following ultraviolet photolysis in a condensed phase environment.[5−9] Among various polyhalomethanes that undergo photoinduced isomerization in the condensed phase, iodoform (CHI_3) has attracted a lot of interest since its synthetic applications have been reported.[10−12] In particular, ultraviolet irradiation of CHI_3 in the presence of olefins yields iodocyclopropanated products. According to DFT calculations, photolysis of CHI_3 yields two types of reaction intermediates, CHI_2 radical and *iso*-CHI_2−I, which can competitively react with olefins to produce iodocyclopropanated products.[13] Interestingly, photolysis of CHI_3 with *trans*- and *cis*-butenes resulted in stereospecific iodocyclopropanated product with no isomerized product being produced from the reaction with *cis*-butene.[12] This finding strongly suggests that *iso*-CHI_2−I is the major agent of iodomethylene transfer,[13] and its asymmetric geometry accounts for stereoselectivity of iodocyclopropanation reaction. Thus, elucidating the photochemistry of CHI_3 and the structure of *iso*-CHI_2−I provides a detailed understanding of how the iodocyclopropanation reaction occurs.

Previous spectroscopic studies have proposed photoreaction pathways of CHI_3 in solution, as summarized in Scheme 1.[13−16] Excitation of CHI_3 at 267 or 350 nm induces the n (X) → σ^* (C−X) transition by which a nonbonding electron localized on a p-orbital of iodine is transferred to an antibonding C−I (σ^*) orbital, producing CHI_2 and I radicals through C−I bond cleavage. The dissociated I radical is expelled from the solvent cage, leaving the CHI_2 radical, or it recombines geminately with the CHI_2 radical in the solvent cage to form *iso*-CHI_2−I. Transient absorption (TA) spectra of CHI_3 in cyclohexane and acetonitrile following excitation at 350 nm showed two transient absorption bands on 10 ps time scale.[15] Those features were assigned to *iso*-CHI_2−I based on time-dependent density functional theory (TDDFT) calculations. Although the spectroscopic evidence of CHI_2 and I radicals was not detected in that study, the presence of the two species cannot be completely ruled out because of the low oscillator strengths of electronic transitions of the two radical species.[15]

Received: November 25, 2017
Accepted: January 16, 2018
Published: January 16, 2018

DOI: 10.1021/acs.jpclett.7b03125
J. Phys. Chem. Lett. 2018, 9, 647−653

Scheme 1. Possible Reaction Pathways for CHI_3 Photolysis in Cyclohexane[a]

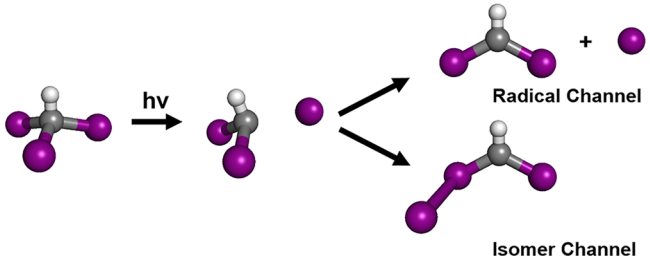

[a]Excitation at 267 nm induces the n (X) → σ^* (C−X) transition, resulting in C−I bond cleavage. The dissociated I radical is expelled from the solvent cage, leaving CHI_2 radical, or it recombines geminately with the CHI_2 radical to form *iso*-CHI_2−I.

Although the previous spectroscopic works provide detailed kinetic traces of *iso*-CHI_2−I,[13−16] the spectroscopic data cannot be used to refine the molecular structure of *iso*-CHI_2−I because the spectroscopic signals in general cannot be accurately calculated from the molecular structure, and thus the structure of the isomer remains elusive. In this regard, time-resolved X-ray solution scattering (TRXSS), also known as time-resolved X-ray liquidography (TRXL), is a relevant tool for probing the structure of the reaction intermediate because it uses X-rays to probe the global structural changes of molecules.[8,17−35] Previously, a TRXL study was performed on the photolysis of CHI_3 in methanol in the time range of 100 ps to 3 μs,[36] but it was not able to confirm the formation of *iso*-CHI_2−I in methanol, due to a low yield of its formation. Instead, the TRXL study showed that CHI_3 dissociates into CHI_2 and I radicals, followed by a nongeminate recombination of two I radicals to form I_2. Thus, to date, the detailed structure of *iso*-CHI_2−I has not been determined.

The lifetime of *iso*-CHI_2−I was measured to be ∼1 μs in cyclohexane.[13,15] By contrast, a femtosecond TA study of CHI_3 in methanol showed that *iso*-CHI_2−I decays rapidly, in only 740 ps, due to insertion of O−H (in methanol) into *iso*-CHI_2−I.[14] These findings imply that *iso*-CHI_2−I is unstable in the polar methanol solvent compared with the nonpolar cyclohexane solvent, suggesting that methanol is not an appropriate solvent for capturing the structure of *iso*-CHI_2−I. Instead, we chose cyclohexane as a solvent to directly observe the structure and kinetic behavior of *iso*-CHI_2−I. In this work, by analyzing our TRXL data using density functional theory (DFT) calculation, molecular dynamics (MD) simulation, and global fit analysis, we present the first demonstration of the detailed structure of *iso*-CHI_2−I and the underlying reaction kinetics of CHI_3 photolysis in cyclohexane.

The experimental and calculated difference scattering curves $q\Delta S(q)$ at various time delays are shown in Figure 1a. The experimental $q\Delta S(q)$ exhibit clear oscillatory features, representing the structural changes of the photoexcited molecules. The calculated $q\Delta S(q)$ were obtained from global fit analysis based on the maximum likelihood estimation (MLE) method, with the reduced-chi square (χ_ν^2) value as a measure of the goodness of the fit.[18−20] In the global fit analysis, the DFT-optimized structures of solute molecules were used as starting structures for the fit and several selected structural parameters of the solute molecules were varied to fit the experimental $q\Delta S(q)$. Specifically, we selected the C−I bond lengths of CHI_3 and CHI_2, I−I bond lengths of I_2 and *iso*-CHI_2−I, and C−I−I bond angle of *iso*-CHI_2−I as fit parameters to refine the actual structure of the chemical species involved in the CHI_3 photolysis. In addition, kinetic parameters such as branching ratios and rate constants were also adjusted in the fit so that the reaction mechanism of CHI_3 photolysis can be determined. The details of the global fit analysis are provided in the Supporting Information (SI).

The best-fit, calculated $q\Delta S(q)$ obtained by the global fit analysis shows good agreement with the experimental $q\Delta S(q)$. The difference radial distribution functions (ΔRDFs), $r^2\Delta R(r)$, where r is the interatomic distance (Figure 1b), were obtained by sine-Fourier-transformation of $q\Delta S(q)$. The ΔRDF signal provides the change in the distribution of interatomic distance, r; thus the positive peak indicates the formation of an atom−atom pair, whereas the negative peak shows disappearance of an atom−atom pair, generally related to bond cleavage. The

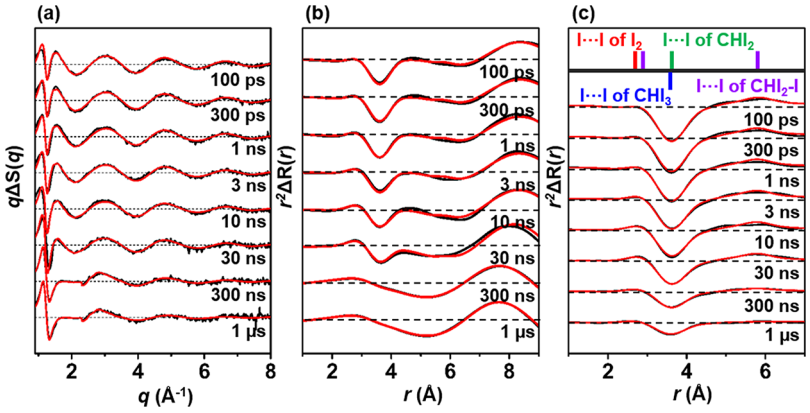

Figure 1. Difference scattering curves, $q\Delta S(q)$ of CHI_3 in cyclohexane as a function of the time delay after excitation at 267 nm. (a) Experimental $q\Delta S(q)$ (black, $q\Delta S(q,t) = qS(q,t) - qS(q, -3\text{ ns})$) and calculated $q\Delta S(q)$ (red) obtained by global fit analysis. For proper comparison of oscillatory features of $q\Delta S(q)$ at 300 ns and 1 μs, $q\Delta S(q)$ below 2.3 Å^{-1} were multiplied by a factor of 0.2. (b) The difference radial distribution functions, $r^2\Delta R(r,t)$ representing the sine-Fourier transformation of $q\Delta S(q,t)$ shown in (a). For proper comparison of peaks of $r^2\Delta R(r,t)$, $r^2\Delta R(r,t)$ at 300 ns and 1 μs were multiplied by a factor of 0.2. (c) The solute-only $r^2\Delta R(r,t)$ from the experiment (black) and from calculation (red). One unit of the y-axis in (b) is 1.5 times of that in (c). The solute-only $r^2\Delta R(r,t)$ was extracted by subtracting the contributions of the cage and the solvent from the $r^2\Delta R(r,t)$. The solute-related atom−atom distances are displayed at the top of the plot. Newly formed atom−atom distances show up as positive peaks, whereas the negative peaks are from depleted atom−atom distances.

DOI: 10.1021/acs.jpclett.7b03125
J. Phys. Chem. Lett. 2018, 9, 647−653

Table 1. List of Structural Parameters of the Chemical Species Involved in CHI3 Photolysis[d]

Species	Parameter	B3LYP/6-311G**[a]	B3LYP/dhf-TZVPP+AVTZ[b]	MN12-SX/dhf-TZVPP+AVTZ[b]	ωB97X/dhf-TZVPP+AVTZ[b]	Expt.[c]
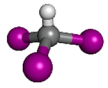	C–I	2.181 Å	2.161 Å	2.133 Å	2.130 Å	2.132 Å (± 0.010)
	I–I	3.641 Å	3.603 Å	3.549 Å	3.545 Å	3.550 Å (± 0.017)
	H–C–I	105.5°	105.7°	106.2°	106.1°	106.1° [Fixed]
	I–C–I	113.2°	113.0°	112.6°	112.7°	112.7° [Fixed]
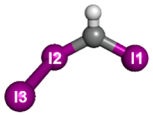	C–I1	2.074 Å	2.062 Å	2.038 Å	2.039 Å	2.039 Å [Fixed]
	C–I2	2.021 Å	2.008 Å	1.977 Å	2.004 Å	2.004 Å [Fixed]
	I1–I3	5.934 Å	5.830 Å	5.724 Å	5.392 Å	5.708 Å (± 0.025)
	I2–I3	3.163 Å	3.087 Å	3.038 Å	3.181 Å	2.922 Å (± 0.004)
	C–I2 –I3	130.2°	130.4°	130.4°	114.2°	133.9° (± 0.8)
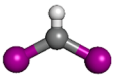	C–I	2.082 Å	2.067 Å	2.048 Å	2.039 Å	2.042 Å (± 0.010)
	I–I	3.677 Å	3.642 Å	3.590 Å	3.599 Å	3.605 Å (± 0.017)
	I–C–I	124.0°	123.5°	122.5°	123.9°	123.9° [Fixed]
	I–C–H	116.2°	116.1°	115.8°	118.0°	118.0° [Fixed]
	I–I	2.738 Å	2.703 Å	2.662 Å	2.662 Å	2.662 Å (± 0.071)

[a]DFT-optimized parameters without considering scalar relativistic effect. [b]DFT-optimized parameters with considering scalar relativistic effect by introducing dhf-TZVPP small-core relativistic effective core potential (RECP) on iodine atom.[37] [c]Errors for global fit parameters are shown in the paranthesis. Fixed values are excerpted from the ωB97X/dhf-TZVPP+AVTZ calculation. [d]The listed parameters were either optimized by DFT calculations or obtained from global fit analysis of the experimental TRXL data. Computational details of the DFT calculations are given in the SI. Additional DFT-optimized structures with different choices of basis sets and functionals are listed in Table S2.

ΔRDF signal shown in Figure 1b is a mixture of three contributions, solute, cage, and solvent, making it difficult to retrieve the change in the solute structure alone. To extract more intuitive structural information from the ΔRDF in Figure 1b, we decomposed it into solute, cage, and solvent contributions (Figure S2). The solute-only ΔRDF in Figure 1c was obtained by subtracting the contributions of the cage and the solvent determined from the best-fit calculated model and represents structural change of reacting solute molecules. From the solute-only ΔRDFs in Figure 1c, we can identify the reaction intermediates and their concentrations as a function of time. By analyzing the change of concentration of each species, we can retrieve the reaction pathways. For example, at 100 ps, three major peaks at 2.8 Å (positive), 3.6 Å (negative), and 5.7 Å (positive) are observed in the solute-only ΔRDF. The strong negative peak at 3.6 Å corresponds to the depletion of the I−I distance in CHI_3 and the positive peaks at 2.8 and 5.7 Å correspond to the formation of the I2−I3 and I1−I3 distances in *iso*-CHI_2−I (Table 1). As the reaction progresses in tens of nanoseconds, the positive peak at 2.8 Å shifts slightly to a shorter distance (∼2.7 Å) and the intensity increases, while the intensity of the positive peak at 5.7 Å remains unchanged. These observations indicate that the concentration of *iso*-CHI_2−I stays constant up to tens of nanoseconds and new iodine-containing species, with atom−atom distances of approximately 2.7 Å, start to form on the nanosecond time scale. The 2.7 Å peak is assigned to formation of I_2 with an I−I distance of 2.662 Å. This peak is not located exactly at 2.662 Å because the I−I distances of *iso*-CHI_2−I (2.922 Å) and I_2 (2.662 Å) both contribute to the peak.

To identify the major intermediates of CHI_3 photolysis on a subnanosecond time scale, we analyzed $q\Delta S(q)$ measured at 100 ps. As shown in Figure 2, we considered three kinetic models of reaction pathways: (1) formation of CHI_2 radical ($CHI_3 \rightarrow CHI_2 + I$), (2) formation of CHI_2−I isomer ($CHI_3 \rightarrow CHI_2$−I), and (3) formation of both CHI_2 radical and

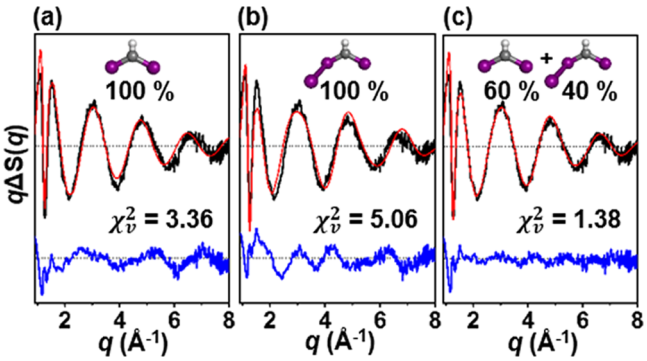

Figure 2. Calculated $q\Delta S(q)$s for the three candidate kinetic models at 100 ps. (a) Direct dissociation into the CHI_2 and I radical ($CHI_3 \rightarrow CHI_2 + I$), (b) CHI_2−I isomer formation ($CHI_3 \rightarrow CHI_2$−I), and (c) the combined model. The experimental (black) and calculated (red) $q\Delta S(q)$ with the residual (blue) obtained by subtracting the two curves (Experiment−Calculation) are shown below. All three panels are on the same scale. Note that the combined model gives the best fit with a radical-to-isomer branching ratio of 60:40.

CHI_2−I isomer with a branching ratio α, $CHI_3 \rightarrow (1 - \alpha)$ (CHI_2 + I) + α CHI_2−I. All of the selected structural parameters were optimized for each kinetic model. As shown in Figure 2, the combined model considering the formation of both CHI_2 radical and CHI_2−I isomer gave the best fit (χ^2_ν = 1.38) with α = 0.40 ± 0.02. The difference in the fit quality between the three kinetic models is clearly visualized in *r*-space by comparing the fits with the solute-only ΔRDF, $r^2\Delta R_{solute}(r)$, as shown in Figure 3. The best-fit model, $CHI_3 \rightarrow$ 60% (CHI_2 + I) + 40% (CHI_2−I), clearly reproduces the three major peaks at 2.8, 3.6, and 5.7 Å in the experimental ΔRDF at 100 ps. The positive peaks at 2.8 and 5.7 Å indicate the formation of new I−I distances and can be assigned to the I2−I3 and I1−I3 distances in *iso*-CHI_2−I, respectively. The $r^2\Delta R_{solute}(r)$ of the radical model has no such positive peaks in the 2−6 Å region

DOI: 10.1021/acs.jpclett.7b03125
J. Phys. Chem. Lett. 2018, 9, 647−653

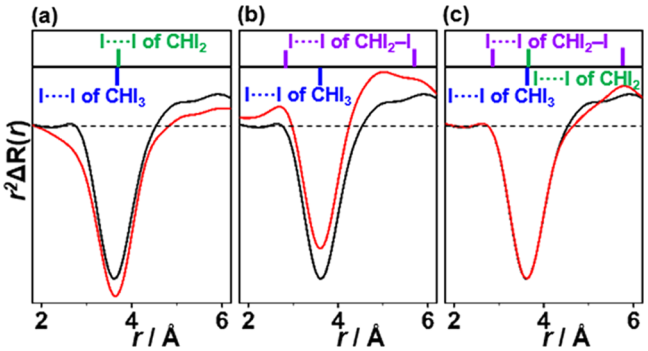

Figure 3. Solute-only ΔRDFs, $r^2\Delta R_{solute}(r)$, for the three candidate models at 100 ps. (a) Radical formation channel, $CHI_3 \rightarrow CHI_2 + I$, (b) isomer formation channel, $CHI_3 \rightarrow CHI_2{-}I$, and (c) the combined model with a radical-to-isomer branching ratio of 60:40. Experimental (black) and calculated (red) $r^2\Delta R_{solute}(r)$ are extracted by subtracting the cage and solvent contributions from the 100 ps experimental and calculated $r^2\Delta R(r)$. All three panels are on the same scale. The solute-related I−I distances from the global fit analysis are displayed at the top of the plots. Newly formed atom−atom distances are associated with in positive peaks; depleted atom−atom distances are negative peaks.

due to the absence of the isomer. On the other hand, the isomer model overestimates $r^2\Delta R_{solute}(r)$ in the two positive peaks, leading to a poor fit. These results strongly indicate that *iso*-CHI_2−I as well as CHI_2 and I radicals are present at 100 ps.

In Table 1, the experimental structures of CHI_3, CHI_2, *iso*-CHI_2−I, and I_2 determined by the global fit analysis of experimental TRXL data are listed in comparison with DFT-optimized structures that were calculated using various basis sets and functionals. In particular, for *iso*-CHI_2−I, the I2−I3 distance (d_{I-I}) and the C−I2−I3 angle (θ_{C-I-I}) were determined to be d_{I-I} = 2.922 ± 0.004 Å and θ_{C-I-I} = 133.9 ± 0.8° from the global fit analysis. We note that, while the DFT-optimized structures for other iodine-containing species (CHI_3, CHI_2, and I_2) do not exhibit much dependence on the calculation method, the DFT-optimized structure of *iso*-CHI_2−I varies sensitively depending on the choice of basis set and functional (Table 1 and Table S2). For example, I2−I3 distance, I1−I3 distance and C−I2−I3 angle vary significantly, from 3.022 to 3.221 Å, 5.392 to 5.934 Å, and 114.2 to 130.4°, respectively, indicating that the DFT calculation cannot predict the consistent molecular structure of *iso*-CHI_2−I. Especially, the structure optimized by MN12-SX/dhf-TZVPP+AVTZ is the closest to the experimental structure, but it still deviates much from the experimental structure. By contrast, the DFT-optimized structures of CHI_3, CHI_2, and I_2 are in good agreement with the experimentally determined structures. Such discrepancy between the experimental and DFT-optimized structures was also observed for *iso*-CH_2I−I generated by another photoreaction, photolysis of CH_2I_2 in cyclohexane,[38−40] and it suggests that the refinement of DFT-optimized structure based on the experimental data is needed for determining the accurate structure of *iso*-CHI_2−I. A more detailed discussion on DFT-optimized structures and their comparison with global-fit structures are given in the SI.

Figure 4 shows the overall reaction mechanism and time-dependent concentration profiles of CHI_3 photolysis in cyclohexane and methanol. Concentration profiles shown in Figure 4c are the optimal concentrations of reaction species in cyclohexane predicted from the optimized kinetic model that best describes the experimental data shown in Figure 1a. Initially, CHI_2 and I radicals are formed by the cleavage of C−I bond in CHI_3, and they undergo two reaction channels: (1) the cage breakout of CHI_2 and I radicals, and (2) the geminate recombination of CHI_2 and I radicals forming *iso*-CHI_2−I, with a branching ratio of 60% and 40%, respectively. Iodine radicals, a product formed after the cage breakout, further undergo nongeminate recombination with I or CHI_2 to form I_2 or CHI_3 with rate constants of 1.52 ± 0.01 × 10^{10} M^{-1} s^{-1} and 7.59 ± 0.01 × 10^9 M^{-1} s^{-1}, respectively. The bimolecular rate constant of I_2 obtained in this TRXL study is consistent with those obtained from previous TRXL and pulse radiolysis studies.[40,41] The concentration of CHI_2 remains constant after 30 ns (when

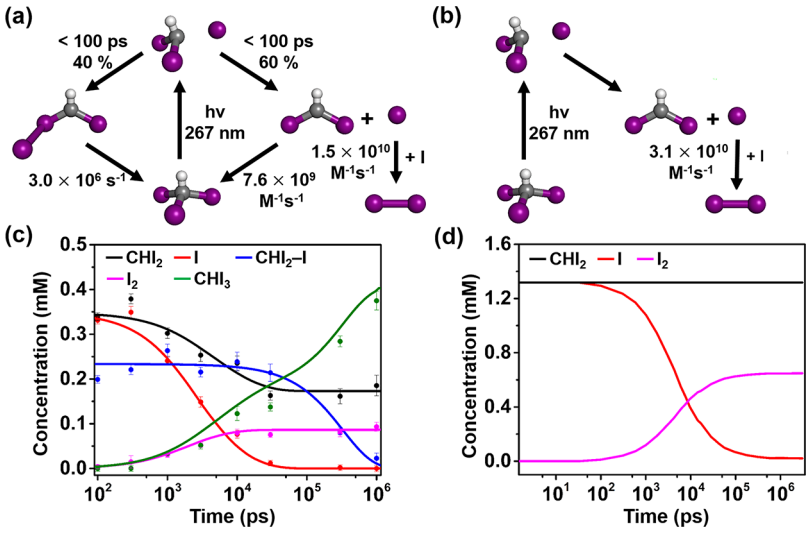

Figure 4. Reaction mechanism of CHI_3 photolysis in (a) cyclohexane determined in this study and (b) methanol from a previous work.[36] The branching ratios and rate constants are shown for each reaction channel. Concentration changes of chemical species involved in CHI_3 photolysis as a function of time delay in (c) cyclohexane and (d) methanol. Solid lines were obtained from optimized global fits based on kinetic models, and symbols were obtained from individual fits of experimental difference scattering curves at various time delays. CHI_3 (olive), CHI_2 radical (black), I radical (red), *iso*-CHI_2−I (blue), and I_2 (magenta).

DOI: 10.1021/acs.jpclett.7b03125
J. Phys. Chem. Lett. 2018, 9, 647−653

most of the I radicals are used up), and the product of $2CHI_2 \rightarrow CHI_2{-}CHI_2$ was not observed in the time range of our measurement.

As noted above, *iso*-$CHI_2{-}I$ is already formed within 100 ps with a quantum yield of ∼40%. The presence of the isomer prior to the formation of I_2 suggests that the isomer is formed by means of geminate recombination within the solvent cage. The geminate recombination rate of *iso*-$CHI_2{-}I$ was not determined in this experiment due to limited temporal resolution of the measurement. The reported recombination time of *iso*-$CHI_2{-}I$ is 7 ps,[14] which is inaccessible with our 100 ps time resolution. The lifetime of *iso*-$CHI_2{-}I$ is 334 ± 5 ns, which is comparable to the value determined from time-resolved TA and resonance Raman experiments.[13−15] It is noteworthy that the reaction pathways of CHI_3 photolysis are much simpler in methanol solvent.[36] As shown in Figures 4b and 4d, CHI_3 in methanol dissociates into CHI_2 and I radicals and subsequent nongeminate recombination of two I radicals produces I_2. In that study, the characteristic I−I distances of *iso*-$CHI_2{-}I$ were not observed in the solute-only ΔRDF at 100 ps, implying that the branching ratio of isomerization in methanol is much lower than that in cyclohexane reported here. The lack of *iso*-$CHI_2{-}I$ in methanol was further confirmed by another study combining TRXL and time-resolved X-ray absorption spectroscopy (TRXAS) measurements, which showed that the major intermediate species of CHI_3 photolysis is CHI_2 and the yield of *iso*-$CHI_2{-}I$ is too low to be detected by those measurements.[42] In methanol, I radicals recombine non-geminately to form I_2 with the bimolecular rate constant of $3.1 \pm 0.5 \times 10^{10}\ M^{-1}\ s^{-1}$, which is twice higher than that in cyclohexane. The higher nongeminate recombination rate of I_2 can be explained by viscosity difference between methanol and cyclohexane. The viscosity of methanol is 0.59 cP, whereas cyclohexane is 1.0 cP, and thus the I radical can diffuse faster in methanol, resulting in the faster nongeminate recombination. Nongeminate recombination rates of I_2 in cyclohexane and methanol determined in the TRXL studies of CHI_3 photolysis are consistent with those reported in previous TRXL studies on different photoreactions involving I radicals.[21] The lifetime (∼330 ns) and quantum yield (∼40%) of *iso*-$CHI_2{-}I$ determined by TRXL is in good agreement with the ones from previous spectroscopic studies.[13−15] However, compared with the previous spectroscopic studies, our TRXL study provides a complete picture of reaction mechanism, without being affected by the absorption strengths of individual chemical species. In those spectroscopic studies, the major spectroscopic features in the TA and resonance Raman spectra were assigned to *iso*-$CHI_2{-}I$ species. The lack of distinct features for the CHI_2 radical in the transient absorption spectra can be attributed to the difference in the oscillator strengths of *iso*-$CHI_2{-}I$ and CHI_2 radical. Kim et al. calculated the oscillator strengths and resonance Raman intensities of the *iso*-$CHI_2{-}I$ and CHI_2 radical in cyclohexane using the same DFT method used in the current study.[42] According to the DFT calculation, the oscillator strength and Raman intensity of *iso*-$CHI_2{-}I$ are 3 orders of magnitude higher than those of CHI_2 radical. This calculation result implies that the TA signal of CHI_2 may be optically "masked" by the intense signal of *iso*-$CHI_2{-}I$. By contrast, TRXL signal contains the contributions of all atomic pairs and therefore CHI_2 radical and *iso*-$CHI_2{-}I$ contribute equally to the X-ray scattering signal, in proportion to their concentrations.

In this work, the photolysis of CHI_3 in cyclohexane with excitation at 267 nm was monitored by time-resolved X-ray solution scattering from 100 ps to 1 μs. The time-dependent scattering signals visualize the structural changes associated with the formation of transient intermediate species. Furthermore, by applying a structural refinement protocol, we determined the three-dimensional structure of *iso*-$CHI_2{-}I$ in solution with atomic spatial resolution. Considering that the DFT-optimized structure of *iso*-$CHI_2{-}I$ varies sensitively depending on the choice of functional and basis set, the experimentally determined structure of *iso*-$CHI_2{-}I$ in this work can be a valuable reference for the development of DFT functional and can give insight into the structural optimization of *iso*-polyhalomethanes by quantum chemical calculations. The structural refinement estimates the geminate recombination probability to be 40%, that is, 60% of the CHI_2 radicals are expelled from the cage at 100 ps. Although it is difficult to probe CHI_2 radicals by optical spectroscopy due to their low oscillator strengths, we were able to determine the kinetics of both *iso*-$CHI_2{-}I$ and CHI_2 from the global fit analysis of TRXL data. Thus, the current TRXL study provides the global reaction mechanism of CHI_3 photolysis.

■ ASSOCIATED CONTENT

Supporting Information

The Supporting Information is available free of charge on the ACS Publications website at DOI: 10.1021/acs.jpclett.7b03125.

The full methods including the DFT calculations, MD simulations, global fit analysis, and TRXL setups (PDF)

■ AUTHOR INFORMATION

Corresponding Author

*E-mail: hyotcherl.ihee@kaist.ac.kr.

ORCID

Joonghan Kim: 0000-0002-7783-0200

Hyotcherl Ihee: 0000-0003-0397-5965

Present Address

[∇]Department of Physics, AlbaNova University Center, Stockholm University, SE-10691 Stockholm, Sweden

Notes

The authors declare no competing financial interest.

■ ACKNOWLEDGMENTS

We acknowledge the initial efforts of D. Suh and S. Cho. This work was supported by Institute for Basic Science (IBS-R004-A1). The TRXL experiment conducted as part of this study was performed at the ID09 beamline in the European Synchrotron Radiation Facility (ESRF).

■ REFERENCES

(1) Blomstrom, D. C.; Herbig, K.; Simmons, H. E. Photolysis of Methylene Iodide in the Presence of Olefins. *J. Org. Chem.* **1965**, *30*, 959−964.

(2) Kropp, P. J. Photobehavior of Alkyl-Halides in Solution - Radical, Carbocation, and Carbene Intermediates. *Acc. Chem. Res.* **1984**, *17*, 131−137.

(3) Kropp, P. J.; Pienta, N. J.; Sawyer, J. A.; Polniaszek, R. P. Photochemistry of Alkyl-Halides 0.7. Cyclopropanation of Alkenes. *Tetrahedron* **1981**, *37*, 3229−3236.

(4) Pienta, N. J.; Kropp, P. J. Photochemistry of Alkyl-Halides 0.6. Gem-Diiodides - Convenient Method for Cyclopropanation of Olefins. *J. Am. Chem. Soc.* **1978**, *100*, 655−656.

DOI: 10.1021/acs.jpclett.7b03125
J. Phys. Chem. Lett. 2018, 9, 647−653

(5) Tarnovsky, A. N.; Alvarez, J. L.; Yartsev, A. P.; Sundstrom, V.; Akesson, E. Photodissociation Dynamics of Diiodomethane in Solution. *Chem. Phys. Lett.* **1999**, *312*, 121−130.
(6) Tarnovsky, A. N.; Pascher, I.; Pascher, T. Reactivity of Iso-Diiodomethane and Iso-Iodoform, Isomers of CH_2I_2 and CHI_3, Toward the Double Bond of a Variety of Cycloalkenes. *J. Phys. Chem. A* **2007**, *111*, 11814−11817.
(7) Zheng, X. M.; Phillips, D. L. Density Functional Theory and Resonance Raman Investigation of the Ultraviolet Electronic Excited States of CF_2I_2. *Chem. Phys. Lett.* **2000**, *316*, 524−530.
(8) Davidsson, J.; Poulsen, J.; Cammarata, M.; Georgiou, P.; Wouts, R.; Katona, G.; Jacobson, F.; Plech, A.; Wulff, M.; Nyman, G.; Neutze, R. Structural Determination of a Transient Isomer of CH_2I_2 by Picosecond X-ray Diffraction. *Phys. Rev. Lett.* **2005**, *94*, 245503.
(9) Preston, T. J.; Shaloski, M. A.; Crim, F. F. Probing the Photoisomerization of $CHBr_3$ and CHI_3 in Solution with Transient Vibrational and Electronic Spectroscopy. *J. Phys. Chem. A* **2013**, *117*, 2899−2907.
(10) Marolewski, T.; Yang, N. Photochemical Addition of Polyhalogenomethanes to Olefins. *Chem. Commun.* **1967**, 1225−1226.
(11) Mielniczak, G.; Bopusinski, A. Iodoform, a New Reagent in the Todd-Atherton Reaction. *Synth. Commun.* **2003**, *33*, 3851−3859.
(12) Yang, N.-C.; Marolewski, T. A. The Addition of Halomethylene to 1, 2-Dimethylcyclobutene, a Methylene-Olefin Reaction Involving a Novel Rearrangement. *J. Am. Chem. Soc.* **1968**, *90*, 5644−5646.
(13) Li, Y. L.; Chen, D. M.; Wang, D. Q.; Phillips, D. L. Time-Resolved Resonance Raman and Density Functional Theory Investigation of Iodocyclopropanation and Addition Reactions with Alkenes after Ultraviolet Photolysis of Iodoform. *J. Org. Chem.* **2002**, *67*, 4228−4235.
(14) El-Khoury, P. Z.; Kwok, W. M.; Guan, X. G.; Ma, C. S.; Phillips, D. L.; Tarnovsky, A. N. Photochemistry of Iodoform in Methanol: Formation and Fate of the Iso-CHI_2-I Photoproduct. *ChemPhysChem* **2009**, *10*, 1895−1900.
(15) Wall, M.; Tarnovsky, A. N.; Pascher, T.; Sundstrom, V.; Akesson, E. Photodissociation Dynamics of Iodoform in Solution. *J. Phys. Chem. A* **2003**, *107*, 211−217.
(16) Zheng, X. M.; Phillips, D. L. Solvation Effects on the Iodoform Ultraviolet Direct Photodissociation Reaction. Opening the Photoisomerization Channel. *Chem. Phys. Lett.* **2000**, *324*, 175−182.
(17) Christensen, M.; Haldrup, K.; Bechgaard, K.; Feidenhans'l, R.; Kong, Q. Y.; Cammarata, M.; Russo, M. L.; Wulff, M.; Harrit, N.; Nielsen, M. M. Time-Resolved X-ray Scattering of an Electronically Excited State in Solution. Structure of the $^3A_{2u}$ State of Tetrakis-μ-pyrophosphitodiplatinate(II). *J. Am. Chem. Soc.* **2009**, *131*, 502−508.
(18) Haldrup, K.; Christensen, M.; Cammarata, M.; Kong, Q. Y.; Wulff, M.; Mariager, S. O.; Bechgaard, K.; Feidenhans'l, R.; Harrit, N.; Nielsen, M. M. Structural Tracking of a Bimolecular Reaction in Solution by Time-Resolved X-Ray Scattering. *Angew. Chem., Int. Ed.* **2009**, *48*, 4180−4184.
(19) Ihee, H.; Lorenc, M.; Kim, T. K.; Kong, Q. Y.; Cammarata, M.; Lee, J. H.; Bratos, S.; Wulff, M. Ultrafast X-ray Diffraction of Transient Molecular Structures in Solution. *Science* **2005**, *309*, 1223−1227.
(20) Jun, S.; Lee, J. H.; Kim, J.; Kim, J.; Kim, K. H.; Kong, Q. Y.; Kim, T. K.; Lo Russo, M.; Wulff, M.; Ihee, H. Photochemistry of $HgBr_2$ in Methanol Investigated Using Time-Resolved X-ray Liquidography. *Phys. Chem. Chem. Phys.* **2010**, *12*, 11536−11547.
(21) Kim, J.; Lee, J. H.; Kim, J.; Jun, S.; Kim, K. H.; Kim, T. W.; Wulff, M.; Ihee, H. Structural Dynamics of 1,2-Diiodoethane in Cyclohexane Probed by Picosecond X-ray Liquidography. *J. Phys. Chem. A* **2012**, *116*, 2713−2722.
(22) Kim, K. H.; Kim, J. G.; Nozawa, S.; Sato, T.; Oang, K. Y.; Kim, T.; Ki, H.; Jo, J.; Park, S.; Song, C.; Sato, T.; Ogawa, K.; Togashi, T.; Tono, K.; Yabashi, M.; Ishikawa, T.; Kim, J.; Ryoo, R.; Kim, J.; Ihee, H.; Adachi, S. Direct Observation of Bond Formation in Solution with Femtosecond X-ray Scattering. *Nature* **2015**, *518*, 385−389.
(23) Kim, K. H.; Oang, K. Y.; Kim, J.; Lee, J. H.; Kim, Y.; Ihee, H. Direct Observation of Myoglobin Structural Dynamics from 100 ps to 1 Microsecond with Picosecond X-ray Solution Scattering. *Chem. Commun.* **2011**, *47*, 289−291.
(24) Kim, T. W.; Lee, J. H.; Choi, J.; Kim, K. H.; van Wilderen, L. J.; Guerin, L.; Kim, Y.; Jung, Y. O.; Yang, C.; Kim, J.; Wulff, M.; van Thor, J. J.; Ihee, H. Protein Structural Dynamics of Photoactive Yellow Protein in Solution Revealed by Pump-Probe X-ray Solution Scattering. *J. Am. Chem. Soc.* **2012**, *134*, 3145−3153.
(25) Kong, Q.; Lee, J. H.; Kim, K. H.; Kim, J.; Wulff, M.; Ihee, H.; Koch, M. H. J. Ultrafast X-ray Solution Scattering Reveals Different Reaction Pathways in the Photolysis of Triruthenium Dodecacarbonyl ($Ru_3(CO)_{12}$) After Ultraviolet and Visible Excitation. *J. Am. Chem. Soc.* **2010**, *132*, 2600−2607.
(26) Lee, J. H.; Kim, T. K.; Kim, J.; Kong, Q.; Cammarata, M.; Lorenc, M.; Wulff, M.; Ihee, H. Capturing Transient Structures in the Elimination Reaction of Haloalkane in Solution by Transient X-ray Diffraction. *J. Am. Chem. Soc.* **2008**, *130*, 5834−5835.
(27) Lee, J. H.; Wulff, M.; Bratos, S.; Petersen, J.; Guerin, L.; Leicknam, J. C.; Cammarata, M.; Kong, Q.; Kim, J.; Moller, K. B.; Ihee, H. Filming the Birth of Molecules and Accompanying Solvent Rearrangement. *J. Am. Chem. Soc.* **2013**, *135*, 3255−3261.
(28) Arnlund, D.; Johansson, L. C.; Wickstrand, C.; Barty, A.; Williams, G. J.; Malmerberg, E.; Davidsson, J.; Milathianaki, D.; DePonte, D. P.; Shoeman, R. L.; Wang, D. J.; James, D.; Katona, G.; Westenhoff, S.; White, T. A.; Aquila, A.; Bari, S.; Berntsen, P.; Bogan, M.; van Driel, T. B.; Doak, R. B.; Kjaer, K. S.; Frank, M.; Fromme, R.; Grotjohann, I.; Henning, R.; Hunter, M. S.; Kirian, R. A.; Kosheleva, I.; Kupitz, C.; Liang, M. N.; Martin, A. V.; Nielsen, M. M.; Messerschmidt, M.; Seibert, M. M.; Sjohamn, J.; Stellato, F.; Weierstall, U.; Zatsepin, N. A.; Spence, J. C. H.; Fromme, P.; Schlichting, I.; Boutet, S.; Groenhof, G.; Chapman, H. N.; Neutze, R. Visualizing a Protein Quake with Time-Resolved X-ray Scattering at a Free-Electron Laser. *Nat. Methods* **2014**, *11*, 923−926.
(29) Biasin, E.; van Driel, T. B.; Kjaer, K. S.; Dohn, A. O.; Christensen, M.; Harlang, T.; Chabera, P.; Liu, Y. Z.; Uhlig, J.; Papai, M.; Nemeth, Z.; Hartsock, R.; Liang, W.; Zhang, J. X.; Alonso-Mori, R.; Chollet, M.; Glownia, J. M.; Nelson, S.; Sokaras, D.; Assefa, T. A.; Britz, A.; Galler, A.; Gawelda, W.; Bressler, C.; Gaffney, K. J.; Lemke, H. T.; Moller, K. B.; Nielsen, M. M.; Sundstrom, V.; Vanko, G.; Warnmark, K.; Canton, S. E.; Haldrup, K. Femtosecond X-Ray Scattering Study of Ultrafast Photoinduced Structural Dynamics in Solvated $[Co(terpy)_2]^{2+}$. *Phys. Rev. Lett.* **2016**, *117*, 013002.
(30) Haldrup, K.; Gawelda, W.; Abela, R.; Alonso-Mori, R.; Bergmann, U.; Bordage, A.; Cammarata, M.; Canton, S. E.; Dohn, A. O.; van Driel, T. B.; Fritz, D. M.; Galler, A.; Glatzel, P.; Harlang, T.; Kjaer, K. S.; Lemke, H. T.; Moller, K. B.; Nemeth, Z.; Papai, M.; Sas, N.; Uhlig, J.; Zhu, D. L.; Vanko, G.; Sundstrom, V.; Nielsen, M. M.; Bressler, C. Observing Solvation Dynamics with Simultaneous Femtosecond X-ray Emission Spectroscopy and X-ray Scattering. *J. Phys. Chem. B* **2016**, *120*, 1158−1168.
(31) Kim, J.; Kim, K. H.; Oang, K. Y.; Lee, J. H.; Hong, K.; Cho, H.; Huse, N.; Schoenlein, R. W.; Kim, T. K.; Ihee, H. Tracking Reaction Dynamics in Solution by Pump-Probe X-ray Absorption Spectroscopy and X-ray Liquidography (Solution Scattering). *Chem. Commun.* **2016**, *52*, 3734−3749.
(32) Plech, A.; Ibrahimkutty, S.; Issenmann, D.; Kotaidis, V.; Siems, A. Ultrafast X-ray Scattering on Nanoparticle Dynamics. *J. Phys.: Conf. Ser.* **2013**, *425*, 092008.
(33) Plech, A.; Randler, R.; Geis, A.; Wulff, M. Diffuse Scattering From Liquid Solutions with White-Beam Undulator Radiation for Photoexcitation Studies. *J. Synchrotron Radiat.* **2002**, *9*, 287−292.
(34) Plech, A.; Kotaidis, V.; Siems, A.; Sztucki, M. Kinetics of the X-ray Induced Gold Nanoparticle Synthesis. *Phys. Chem. Chem. Phys.* **2008**, *10*, 3888−3894.
(35) Kim, T. K.; Lee, J. H.; Wulff, M.; Kong, Q.; Ihee, H. Spatiotemporal Kinetics in Solution Studied by Time-Resolved X-Ray Liquidography (Solution Scattering). *ChemPhysChem* **2009**, *10*, 1958−1980.
(36) Lee, J. H.; Kim, J.; Cammarata, M.; Kong, Q.; Kim, K. H.; Choi, J.; Kim, T. K.; Wulff, M.; Ihee, H. Transient X-ray Diffraction Reveals

DOI: 10.1021/acs.jpclett.7b03125
J. Phys. Chem. Lett. 2018, 9, 647−653

Global and Major Reaction Pathways for the Photolysis of Iodoform in Solution. *Angew. Chem., Int. Ed.* **2008**, *47*, 1047−1050.
(37) Weigend, F.; Baldes, A. Segmented Contracted Basis Sets for One- and Two-Component Dirac-Fock Effective Core Potentials. *J. Chem. Phys.* **2010**, *133*, 174102.
(38) Zheng, X. M.; Phillips, D. L. Solvation can Open the Photoisomerization Pathway for the Direct Photodissociation Reaction of Diiodomethane: Transient Resonance Raman Observation of the Isodiiodomethane Photoproduct from Ultraviolet Excitation of Diiodomethane in the Solution Phase. *J. Phys. Chem. A* **2000**, *104*, 6880−6886.
(39) Phillips, D. L.; Fang, W. H. Density Functional Theory Investigation of the Reactions of Isodihalomethanes (CH2X-X where X = Cl, Br, or I) with Ethylene: Substituent Effects on the Carbenoid Behavior of the CH2X-X Species. *J. Org. Chem.* **2001**, *66*, 5890−5896.
(40) Vincent, J.; Andersson, M.; Eklund, M.; Wöhri, A. B.; Odelius, M.; Malmerberg, E.; Kong, Q.; Wulff, M.; Neutze, R.; Davidsson, J. Solvent Dependent Structural Perturbations of Chemical Reaction Intermediates Visualized by Time-Resolved X-ray Diffraction. *J. Chem. Phys.* **2009**, *130*, 154502.
(41) Foldiak, G.; Schuler, R. H. Rate Constants for Scavenging of Radicals by Iodine. *J. Phys. Chem.* **1978**, *82*, 2756−2757.
(42) Kim, K. H.; Kim, J.; Oang, K. Y.; Lee, J. H.; Grolimund, D.; Milne, C. J.; Penfold, T. J.; Johnson, S. L.; Galler, A.; Kim, T. W.; Kim, J. G.; Suh, D.; Moon, J.; Kim, J.; Hong, K.; Guerin, L.; Kim, T. K.; Wulff, M.; Bressler, C.; Ihee, H. Identifying the Major Intermediate Species by Combining Time-Resolved X-ray Solution Scattering and X-ray Absorption Spectroscopy. *Phys. Chem. Chem. Phys.* **2015**, *17*, 23298−23302.

DOI: 10.1021/acs.jpclett.7b03125
J. Phys. Chem. Lett. 2018, 9, 647−653